ResearchGate

See discussions, stats, and author profiles for this publication at: https://www.researchgate.net/publication/260425392

Thermogravimetric Analysis of Activated Carbons, Ordered Mesoporous Carbide-Derived Carbons, and Their Deactivation Kinetics of Catalytic Methane Decomposition

ARTICLE *in* JOURNAL OF INDUSTRIAL AND ENGINEERING CHEMISTRY · FEBRUARY 2014

Impact Factor: 3.51 · DOI: 10.1021/ie402195q

CITATIONS
4

READS
77

6 AUTHORS, INCLUDING:

Nesrin Ozalp
University of Leuven
43 PUBLICATIONS **345** CITATIONS
SEE PROFILE

Martin Oschatz
Utrecht University
56 PUBLICATIONS **999** CITATIONS
SEE PROFILE

Lars Borchardt
Technische Universität Dresden
62 PUBLICATIONS **1,516** CITATIONS
SEE PROFILE

Stefan Kaskel
Technische Universität Dresden
295 PUBLICATIONS **6,802** CITATIONS
SEE PROFILE

Available from: Nesrin Ozalp
Retrieved on: 30 January 2016

I&EC research
Industrial & Engineering Chemistry Research

Article

pubs.acs.org/IECR

Thermogravimetric Analysis of Activated Carbons, Ordered Mesoporous Carbide-Derived Carbons, and Their Deactivation Kinetics of Catalytic Methane Decomposition

Vidyasagar Shilapuram,[†] Nesrin Ozalp,*[,†] Martin Oschatz,[‡] Lars Borchardt,[‡] Stefan Kaskel,[§] and Robert Lachance[†]

[†]Mechanical Engineering Department, Texas A&M University at Qatar, P.O. Box 23874, Doha, Qatar

[‡]Department of Inorganic Chemistry, Dresden University of Technology, Dresden 01069, Germany

[§]Department of Chemical Surface and Reaction Technology, Fraunhofer Institute for Material and Beam Technology IWS, Dresden 01277, Germany

ABSTRACT: This study presents the deactivation kinetics of methane decomposition for the activated carbons Fluka-05105 and Fluka-05120, ordered mesoporous carbon (CMK-3), and ordered mesoporous carbide-derived carbon (DUT-19). The experimental and thermodynamically predicted carbon deposition, the average and total hydrogen production, and the effect of flow rate on carbon formation rate of these catalysts were investigated. Results indicate that the experimental conditions chosen were within the reaction control regime. Catalytic activity was calculated via two different definitions present in literature: one in terms of carbon deposition rate and the other in terms of carbon mass deposited. Deactivation kinetics were obtained by fitting the experimental data by nonlinear regression analysis. Differences between the two methods in determining activity resulted in significant changes in the estimation of deactivation kinetics. The activity calculated based on the rate method results in the best fit of experimentally collected data. A deactivation order and methane concentration dependency of approximately 1.0 and 0.5 were determined for all the catalysts tested (Fluka-05105, Fluka-05120, CMK-3, and DUT-19). The activation energy of deactivation (E_d) was determined to be 192, 154, 166, and 181 kJ/mol for Fluka-05120, Fluka-05105, CMK-3, and DUT-19, respectively. DUT-19 was the best performing catalyst in terms of carbon formation rate, total carbon production, hydrogen production rate, average hydrogen production, and total hydrogen production.

1. INTRODUCTION

Hydrogen is a promising fuel because it has a high heating value and water vapor is the only product of its combustion.[1] These characteristics attract researchers concerned with the effects of climate change due to CO_2 emission. As a result, various hydrogen processing and production technologies are in development to utilize it as feedstock and develop different production scales.[2] In industry, hydrogen is typically produced by steam reforming of methane, resulting in hydrogen and carbon dioxide product gases. Hydrogen as a product of steam reforming of methane requires carbon dioxide separation before hydrogen can be used as a fuel or feedstock, increasing the energy intensity and carbon footprint of the process. Therefore, an alternative process that is less energy intensive with a lower CO_2 output would be beneficial to both industry and the environment.

One such application for hydrogen production is solar thermal natural gas cracking. In this process, solar energy is concentrated and used as process heat to create hydrogen and solid carbon. Solar cracking of natural gas is an attractive option in the transition from hydrocarbon-dependent processes to renewable energy-based processes.[3] The products of solar cracking of natural gas are both valuable; hydrogen can be combusted as a fuel source or used as a feedstock and carbon can be used as a fuel or material commodity. Although natural gas is used as a feedstock of the solar cracking, no CO_2 emission is created as a product of the process. Solar thermal natural gas cracking allows the separation of carbon in the solid phase, completely eliminating the need for CO_2 capture, storage, and transportation.

In order to design a reactor to house solar cracking of natural gas, kinetics, heat transfer, and reactant flow patterns must be studied and optimized concurrently. Kinetics studies can be conducted using a lab scale reactor in order to optimize input and operation parameters for the design of commercial reactors. Thermodynamics of methane decomposition shows that noncatalytic methane decomposition requires temperatures above 1200 °C for complete decomposition of methane into hydrogen and carbon.[8] In the past, various transition metal and carbonaceous catalysts have been investigated to test their impact on methane decomposition.[9−13] However, metal catalysts tend to rapidly deactivate and their regeneration requires a reactor shutdown. As a result, researchers have most recently focused on carbon-based catalysts because they do not require further separation from the product carbon, they are much less expensive than metal catalysts, regeneration is not

Special Issue: Recent Advances in Natural Gas Conversion

Received: July 12, 2013
Revised: September 18, 2013
Accepted: September 18, 2013
Published: September 18, 2013

ACS Publications © 2013 American Chemical Society

dx.doi.org/10.1021/ie402195q | Ind. Eng. Chem. Res. 2014, 53, 1741−1753

required, and replacing catalyst in a fluidized reactor does not require a reactor shutdown.

This study examines the catalytic behavior of the various carbonaceous catalysts for methane decomposition using a thermogravimetric analyzer (TGA). In literature, carbons of either commercial or synthesized origin with various crystallographic and surface structures were used as catalysts by many research groups for methane decomposition.[14−21] Muradov's group has initiated and made significant contributions to the field of catalytic decomposition of methane using various carbonaceous catalysts in different reactor types.[22−24]

Thermogravimetric analysis is considered advantageous over laboratory-scale reactors in finding the kinetics because of its ability to measure the changes of mass with time and of catalytic activity as the carbon deposits and the requirement of only a small amount of catalyst.[25] This study focuses on thermogravimetric analysis of methane decomposition using various catalysts to obtain the kinetics and deactivation parameters of the process. The paper examines methane decomposition at various temperatures and methane partial pressures with the use of Fluka-05120, Fluka-05105, CMK-3, and DUT-19 catalysts. The effect of flow rate, catalytic activity, hydrogen production, carbon weight gain, and deactivation kinetics were determined.

Similar research on carbonaceous catalytic methane decomposition was previously carried out via thermogravimetic analysis by Abbas et al.[25−27] Palm-shell-based activated carbon (ACPS) manufactured from palm oil shells of various particle sizes as well as commercial-based activated carbon (AC Norit) were used as catalysts for methane decomposition.[25] Results showed a reaction order of 0.5, and activation energy of 210 kJ/mol was obtained for both catalysts. For the same ACPS sample tested with a fixed bed reactor, Abbas and Daud[26] observed a reaction order of 2 and an activation energy of 163 kJ/mol for ACPS catalyst. The reason for this difference was determined to be either large sample mass creating a gradient in methane partial pressure from the bulk gas to the catalyst surface or the method of calculation.

Abbas and Daud[27] studied the deactivation kinetics with ACPS samples and the results showed a deactivation order of 0.5 and a deactivation energy of 194 kJ/mol for ACPS. A comparison of activated carbon samples obtained from palm oil shell (ACPS) and another commercial activated carbon (AC norit) showed similar deactivation kinetics. XRD results showed that fresh ACPS has a higher degree of disorder than the other catalysts tested and also displayed higher catalytic activity during experimentation. Carbon deposition on the catalyst was observed to decrease the degree of disorder and decrease the activity of the sample. An increase in reaction temperature was also observed to decrease the degree of disorder. Relatively disordered amorphous carbons were observed to be highly catalytically active compared to ordered turbostatic and graphitic carbon.[26,27] The initial rate of methane decomposition was modeled using the effect of process parameters by two statistical analysis approaches: (1) a factorial design method and (2) an analysis of variance (ANOVA).[28] The factorial design results showed temperature has a larger effect on carbon deposition rate than feed gas methane partial pressure. ANOVA results determined catalyst weight has a more significant effect than temperature on the initial rate of methane decomposition.

Methane decomposition using carbonaceous catalysts was also studied by Pinilla et al.[29] and Suelves et al.[30] Results show that the reaction order was 0.5 for both samples. Activation energies were determined to be 141 and 238 kJ/mol for CG Norit and BP2000, respectively. Methane decomposition was controlled by two simultaneous processes: (1) decreases in methane decomposition due to active sites being blocked by the deposition of formed carbon and (2) an increase in methane decomposition due to the formation of catalytically active carbon produced from methane decomposition. Suelves et al.[30] studied the thermocatalytic decomposition of methane in a TGA using a wide range of carbon blacks and commercially available activated carbon with different textural properties and surface chemistry. Results show that commercially available carbon black (BP2000) has the highest capacity of carbon accumulation, with 6.13 g deposition/gram of catalyst.

Serrano et al.[31−33] and Botas et al.[34,35] also investigated methane decomposition using synthesized ordered mesoporous carbons CMK-3 and CMK-5 in addition to commercially available activated carbon. The results showed that CMK-5 has higher reaction rates compared to those of CMK-3 and activated carbon. Higher hydrogen production rates were obtained from the synthesized mesoporous carbon samples CMK-3 and CMK-5 as a result of exceptional activity and stability due to their high surface area and bimodal mesopore system. Botas et al.[31] observed that CMK-5 still retains some catalytic activity with 25 g of carbon deposited per gram of catalyst after 72 h of reaction at 950 °C. Further work measured 31 and 15 g of carbon deposited per gram of CMK-5 and CMK-3 catalyst, respectively, at a reaction temperature of 990 °C for 72 h.[32]

Ozalp and Shilapuram previously studied the catalytic characteristics of activated carbons Fluka-05105 and Fluka-05120 for methane decomposition in a thermogravimetric analyzer.[36,37] A higher threshold temperature was observed for Fluka-05120. Under the same reaction temperature and methane partial pressure conditions, higher hydrogen production and carbon weight gain with higher catalytic performance was observed for Fluka-05105 compared to Fluka-05120. Shilapuram et al.[38] also studied the catalytic activity of in house synthesized CMK-3 and DUT-19 to obtain methane decomposition reaction kinetics. These ordered mesoporous/nanoporous carbons were determined to have better catalytic performance for methane decomposition than commercially available carbons.

Recent studies show that hierarchical ordered meso- and microporous carbons are of growing importance, and they find applications in various other fields.[39] It is seen that the mesoporous/nanoporous carbons to have better performance in applications such as high pressure gas storage, energy storage, and lithium storage than current best practices.[40−42] Furthermore, it has been observed that carbonaceous materials also have improved heat transfer characteristics for reactor applications in addition to high reaction rates.[43] This paper furthers the literature concerning carbonaceous catalysts for methane cracking by examining methane decomposition at various temperatures and methane partial pressures with Fluka-05120, Fluka-05105, CMK-3, and DUT-19. The effect of flow rate, catalytic activity, hydrogen production, carbon weight gain, and deactivation kinetics were determined for these catalysts and presented in this paper.

2. EXPERIMENTAL METHODOLOGY

Methane decomposition experiments were performed in a thermogravimetric analyzer (Setsys Evolution 16/18, M/s;

dx.doi.org/10.1021/ie402195q | Ind. Eng. Chem. Res. 2014, 53, 1741−1753

Setaram Instrumentation, France). In the thermogravimetric analyzer, methane is decomposed into hydrogen gas and solid carbon. Hydrogen exits the TGA, and carbon is deposited on the catalyst surface. The TGA records an increase in the mass of catalyst sample over the course of the reaction as a result of this deposition. The crucible used in these experiments was made of 10% Pt−Rh alloy with a 130 μL volume.

A catalyst sample of known mass was loaded into the crucible and deposited in the furnace. Air introduced into the reaction chamber as a result of sample loading was purged by applying a vacuum followed by filling the reaction chamber with a carrier gas (He). This procedure was repeated three times after each sample introduction in order to avoid oxidizing the catalyst or feed gas upon reaching high temperature. The temperature program of the experiment consisted of three zones. In the first zone, carrier gas flow was set with a temperature ramp rate of 30 °C/min until achieving the desired reaction temperature. Carrier gas continued to flow for 15 min to ensure the reactor temperature was stable and allow any gases adsorbed on the catalyst during sample introduction to desorb. In the second zone, auxiliary gas (CH_4) with the methane partial pressure of interest was then introduced into the furnace while simultaneously adjusting the carrier gas flow rate. The reaction was allowed to proceed for the time period of interest. Automated data acquisition allowed high data resolution over 6 and 24 h reaction periods as shown in Table 1. In the final zone, auxiliary gas flow was replaced by carrier gas flow and the furnace was allowed to cool to ambient temperatures.

This procedure was adopted for the various reaction temperatures and inlet mole fractions of methane shown in Table 1 for each catalyst. Experiments were conducted at a total flow rate of 20, 40, and 100 mL/min with a methane feed gas mole fraction varying from 0.1 to 0.5. The reaction temperatures investigated were 950, 880, and 780 °C. The resulting details are presented in Table 1. Experimental conditions were selected such that the effect of flow rate, temperature, carbon weight gain, hydrogen production, deactivation kinetics with each catalyst could be studied and compared. The catalytic properties of the catalysts studied is shown in Table 2.

3. RESULTS AND DISCUSSION

3.1. Effect of Flow Rate. The amount of carbon deposited and the derivative of carbon deposition with respect to time were observed and recorded. From this data, the carbon formation rate was calculated as the ratio of the derivative of carbon weight gain per initial amount of catalyst sample mass. In this study, the carbon formation rate or carbon deposition rate is termed reaction rate. Mass gain and weight gain are defined as the amount of carbon formed per amount of initial catalyst sample. Figure 1 shows the carbon formation rate as a function of time. At each flow rate, the maximum carbon formation rate occurs within a few minutes after the methane decomposition reaction begins. These initial carbon formation rates vary among the catalysts and flow rates. Exceptionally high initial reaction rates were observed with CMK-3 and DUT-19 compared to those of commercially available activated carbons.

Across the panels in Figure 1, it can be observed that the reaction rate dropped with time as a result of deactivation, immaterial of reaction conditions or the nature of catalytic material. Additionally, the trend of reaction rate drop was similar for all of the carbonaceous catalysts. Initially, the reaction rate drops quickly, and it then transitions to a steady reaction rate close to zero. The trend of carbon formation rate

Table 1. Experimentally Observed Carbon Formation for the Chosen Reaction Conditions

run no.	name of the catalyst	temperature, °C	auxiliary gas flow rate (CH_4), mL/min	total flow rate (CH_4+He), mL/min	experimental observation of carbon formed (initial weight of catalyst), mg
1[a]	Fluka-05105	950	10	40	12.8 (11.1)
2[a]	Fluka-05105	950	5	20	15.80 (11.8)
3[a]	Fluka-05105	900	10	40	9.14 (10.8)
4[a]	Fluka-05105	900	5	20	9.98 (12)
5[a]	Fluka-05105	850	10	40	5.78 (8.20)
6[a]	Fluka-05105	850	5	20	7.94 (11.8)
7[a]	Fluka-05105	950	10	20	22.12 (11.3)
8[a]	Fluka-05120	950	10	20	18.14 (16.2)
9[a]	Fluka-05120	950	10	40	11.95 (16.5)
10[a]	Fluka-05120	950	5	20	18.45 (16.3)
11	CMK-3	950	10	100	15.96 (6.2)
12	CMK-3	950	2	20	17.21 (6.2)
13	CMK-3	950	5	20	27.88 (4.9)
14	CMK-3	950	10	20	49.16 (5.4)
15	CMK-3	880	2	20	7.38 (5.6)
16	CMK-3	880	5	20	9.69 (6.5)
17	CMK-3	880	10	20	13.44 (7)
18	CMK-3	780	2	20	5.02 (5.2)
19	CMK-3	780	5	20	7.47 (7.1)
20	CMK-3	780	10	20	6.18 (4.5)
21	DUT-19	950	10	100	14.55 (4.1)
22	DUT-19	950	2	20	14.00 (3.7)
23	DUT-19	950	5	20	24.39 (4.1)
24	DUT-19	950	10	20	35.01 (4.6)
25	DUT-19	880	2	20	9.91 (3.9)
26	DUT-19	880	5	20	10.72 (3.9)
27	DUT-19	880	10	20	13.95 (4.3)
28	DUT-19	780	2	20	6.01 (4.2)
29	DUT-19	780	5	20	8.55 (4.2)
30	DUT-19	780	10	20	11.49 (5.0)

[a]Denotes 6 h of methane decomposition reaction for run numbers 1−10. The remainder of the experiments have a duration of 24 h.

can be divided into two zones of different reaction rate behavior. In the initial zone, the reaction rate decreases at a large rate. This can be explained by rapid carbon deposition in the pore systems of the catalysts. The initial reaction rate was also higher with a higher flow rate due to more rapid carbon deposition in the catalysts' pore systems. It was observed that after some particular time, reaction rates converge to a constant value regardless of flow rate for all catalysts tested. The value to which the reaction rate converges in the final zone at high and

dx.doi.org/10.1021/ie402195q | Ind. Eng. Chem. Res. 2014, 53, 1741−1753

Table 2. Catalytic Properties of the Catalysts Chosen for Methane Decomposition Study

catalyst	particle size (μm)	surface area (m^2/g)	commercial/ synthesized
Fluka-05120	891.6	46.1	commercial
Fluka-05105	890.1	33.6	commercial
CMK-3	1400	*a*	synthesized
DUT-19	2420	*a*	synthesized

[a]Synthesized catalyst amount was very small; hence, particle size analysis data is not provided.

low flow rate converges for Fluka-05105, CMK-3, and DUT-19 because of the complete filling of the carbons pore systems with deposited carbon. In consequence, only external particle surfaces are available for carbon deposition, significantly lowering the catalytic activity. For the variables examined, the condition that had the largest bearing on the rate of carbon deposition was temperature. As temperature increased, a higher carbon deposition rate was observed, corresponding to a higher reaction rate and confirming that the catalytic reaction was in a kinetically controlled regime.[44] The particle size of catalysts chosen in the present study was less than those used by the Kim et al.[45] and Abbas and Daud,[25] where they had assumed the intraparticle mass transfer effects were negligible and diffusional control can be ruled out under the chosen conditions. Furthermore, no film mass transfer exists because all of the catalysts chosen were porous.[46] This evidence further confirms that catalytic system was reaction-controlled.

Figure 2 shows the effect of flow rate on carbon weight gain ($C_{dep}/C_{catalyst}$), defined as the mass of carbon formed as a result of methane decomposition per initial catalyst mass. A two zone phenomena was observed with respect to catalyst weight. This is expected, as catalyst weight gain is a result of reaction rate, which also showed a two zone phenomena. At 950 °C, Fluka-05105, CMK-3, and DUT-19 had more initial carbon deposition at higher flow rates because the reaction is kinetically controlled. After a particular length of time, the rate at which carbon deposits decreased below that of the low flow condition. Therefore, more carbon weight gain was observed with the lower flow rate due to the reaction duration chosen. At lower temperatures (850 and 900 °C), the carbon formation rates were lower compared to the reaction rate at 950 °C, resulting in a slower carbon deposition and deactivation rate. As a result, the number of active sites were depleted at a slower rate. Therefore, at lower temperatures, the higher the flow rate, the higher the carbon weight gain observed. The carbon weight deposited with time (Figure 2) was in agreement with carbon formation rate with time as shown in Figure 1. This shows flow rate, in addition to reaction temperature, and carbon deposition effect as controlling resistances during the course of the methane decomposition process. For Fluka-05120 in Figure 2c, the mass of carbon deposited and the carbon formation rate were larger at lower flow rates compared to higher flow rates. Upon comparison of Figures 1a–d and 2a–d, results show that higher reactions rates were obtained with Fluka-05105 compared to Fluka-05120 for the same experimental conditions. This is in agreement with work done by Shilapuram and Ozalp.[37]

3.2. Comparison of Catalysts for Carbon Weight Gain, Carbon Formation Rate, Total Hydrogen Production, and Average Hydrogen Production. Figure 3 shows the carbon weight gain for different carbonaceous catalysts at 950 °C, methane partial pressure of 0.5, and total flow rate of 20 mL/min. The corresponding carbon formation rate is shown in Figure 4. With Fluka-05120 and Fluka-05105, experiments were conducted for 6 h, whereas for CMK-3 and DUT-19 experiments were conducted for 24 h. Figures 3 and 4 show that the amount of carbon deposition was highest for DUT-19, followed by CMK-3, Fluka-05105, and Fluka-05120 corresponding to the pore volume available for carbon deposition. Equivalently, DUT-19 has a higher reaction rate than CMK-3, Fluka-05105, and Fluka-05120. From Figure 4, it can be observed that the carbon formation rate approaches a constant value for all four carbon samples 5000 s after reaction initialization. Therefore, the average carbon formation rate can be calculated from 5000 s to the end of the reaction. The average carbon formation rates were 0.005, 0.0056, 0.0037, and 0.002 $mg_{carbon}\ mg_{catalyst}^{-1}\ min^{-1}$ for DUT-19, CMK-3, Fluka-05105, and Fluka- 05120, respectively.

BET surface area and XRD results showed that Fluka-05105 and Fluka-05120 contain microporous and amorphous carbon. Small angle X-ray scattering results showed that CMK-3 and DUT-19 were determined to be of amorphous and mesoporous material. The surface areas of CMK-3 and DUT-19 were higher than that of Fluka samples.[38] Total surface areas measured by Shilapuram et al.[37] for Fluka-05105 and Fluka-05120 were 890 and 892 m^2/g, respectively. The particle size of Fluka-05105 was 33.6 μm, whereas the particle size for Fluka-05120 was 46.1 μm. Although the surface areas of the two materials are the same, it is possible that the utilization of the active sites was lower for Fluka-05120 because a larger percentage of sites within the particle become blocked by surface agglomeration. Therefore, particle size effect is reflected in catalytic performance, showing that Fluka-05105 performs better than Fluka-05120 in methane decomposition.

An experimental study of Kim et al. shows that no intermediate gases were formed during the methane decomposition where hydrogen remains as the only product gas. Also, a thermodynamic analysis by Yoon et al.[47] shows that hydrogen is the only product gas for the reaction at temperatures below 1400 K. In this study, the hydrogen production rate was calculated from the stoichiometric balance of methane decomposition assuming only carbon and hydrogen were produced. Total hydrogen production at the end of each reaction was calculated by summing over the instantaneous hydrogen produced. Table 3 shows the total and average hydrogen production of each catalyst for both methane partial pressures at a reaction temperature of 950 °C. Results show that the total and average hydrogen production varied with each catalyst, corresponding to the variation in the molar carbon formation rate of each catalyst. The highest hydrogen production was observed with DUT-19, very closely followed by CMK-3. The reason for increased hydrogen production of the synthetic carbons may due to the presence of additional mesopores and higher surface areas compared to the Fluka samples.

Approximately 1.5 to 2 times the total and average hydrogen production was observed with DUT-19 and CMK-3 compared to that of Fluka-05105, whereas more than 3 times the total and average hydrogen production was observed compared to that observed with Fluka-05120.

A two zone phenomena in carbon weight gain or carbon formation rate with time was observed for all catalysts. In the first zone, the carbon weight gain increases and the carbon formation rate decreases more rapidly with time. In the second

dx.doi.org/10.1021/ie402195q | Ind. Eng. Chem. Res. 2014, 53, 1741–1753

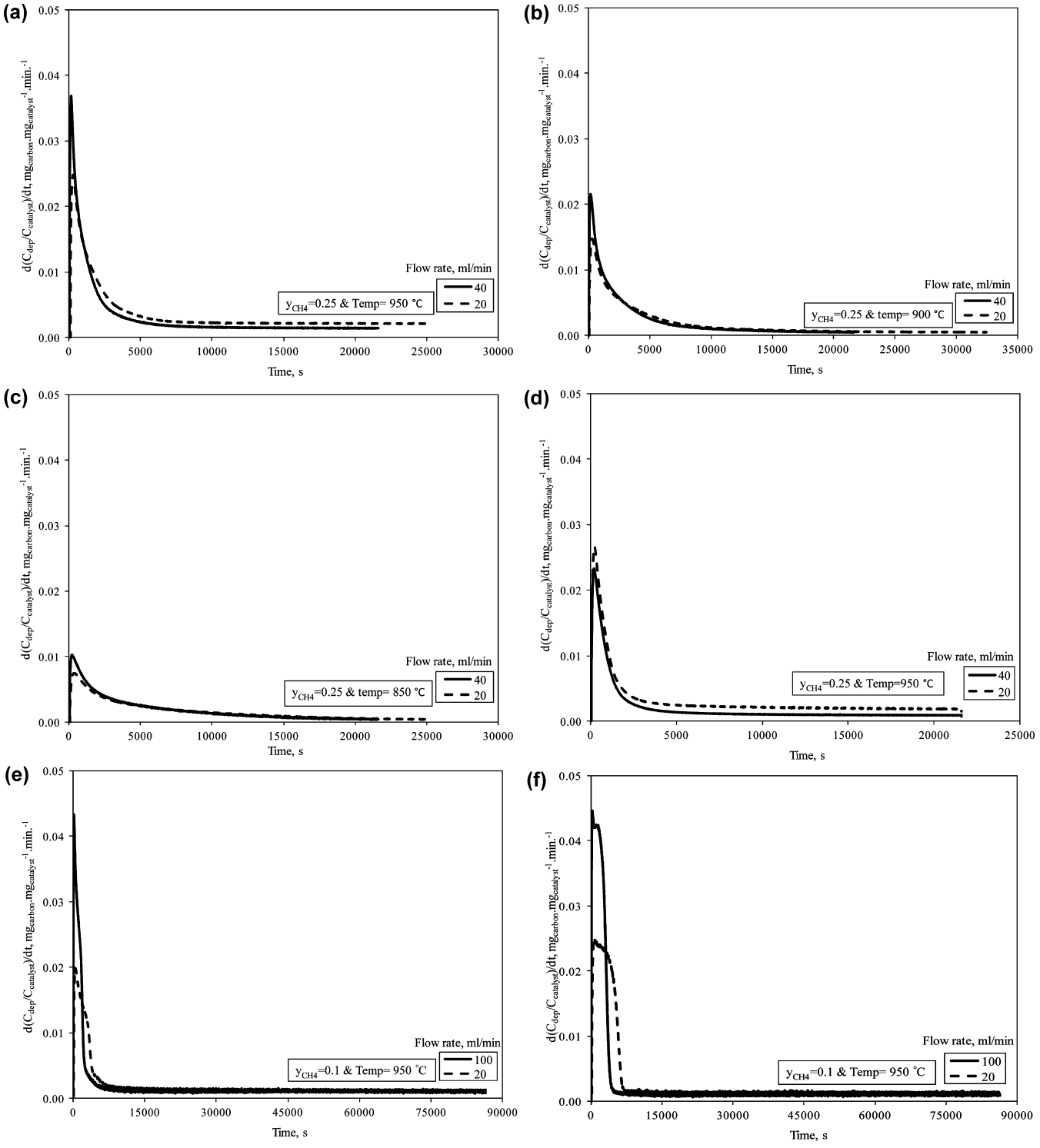

Figure 1. (a) Effect of flow rate on carbon formation rate with Fluka-05105 catalyst. (b) Effect of flow rate on carbon formation rate with Fluka-05105 catalyst. (c) Effect of flow rate on carbon formation rate with Fluka-05105 catalyst. (d) Effect of flow rate on carbon formation rate with Fluka-05120 catalyst. (e) Effect of flow rate on carbon formation rate with CMK-3 catalyst. (f) Effect of flow rate on carbon formation rate with DUT-19 catalyst.

zone, the change in carbon weight gain and carbon formation rate was extensively reduced. Though the change in carbon formation rate in the second zone was reduced with all the catalysts, the comparison shows that a higher carbon formation rate was possible with CMK-3 and DUT-19 catalysts compared to Fluka samples. After 24 h of reaction with DUT-19 and CMK-3, a significant average and total hydrogen production is observed, as shown in Table 3.

Figures 3 and 4 show that the carbon formation rate for DUT-19 and CMK-3 intersected after approximately 1 h of operation. A similar profile was also observed in terms of ultimate weight gain versus time for DUT-19 and CMK-3. However, the point of intersection of weight gain occurred after

dx.doi.org/10.1021/ie402195q | Ind. Eng. Chem. Res. 2014, 53, 1741−1753

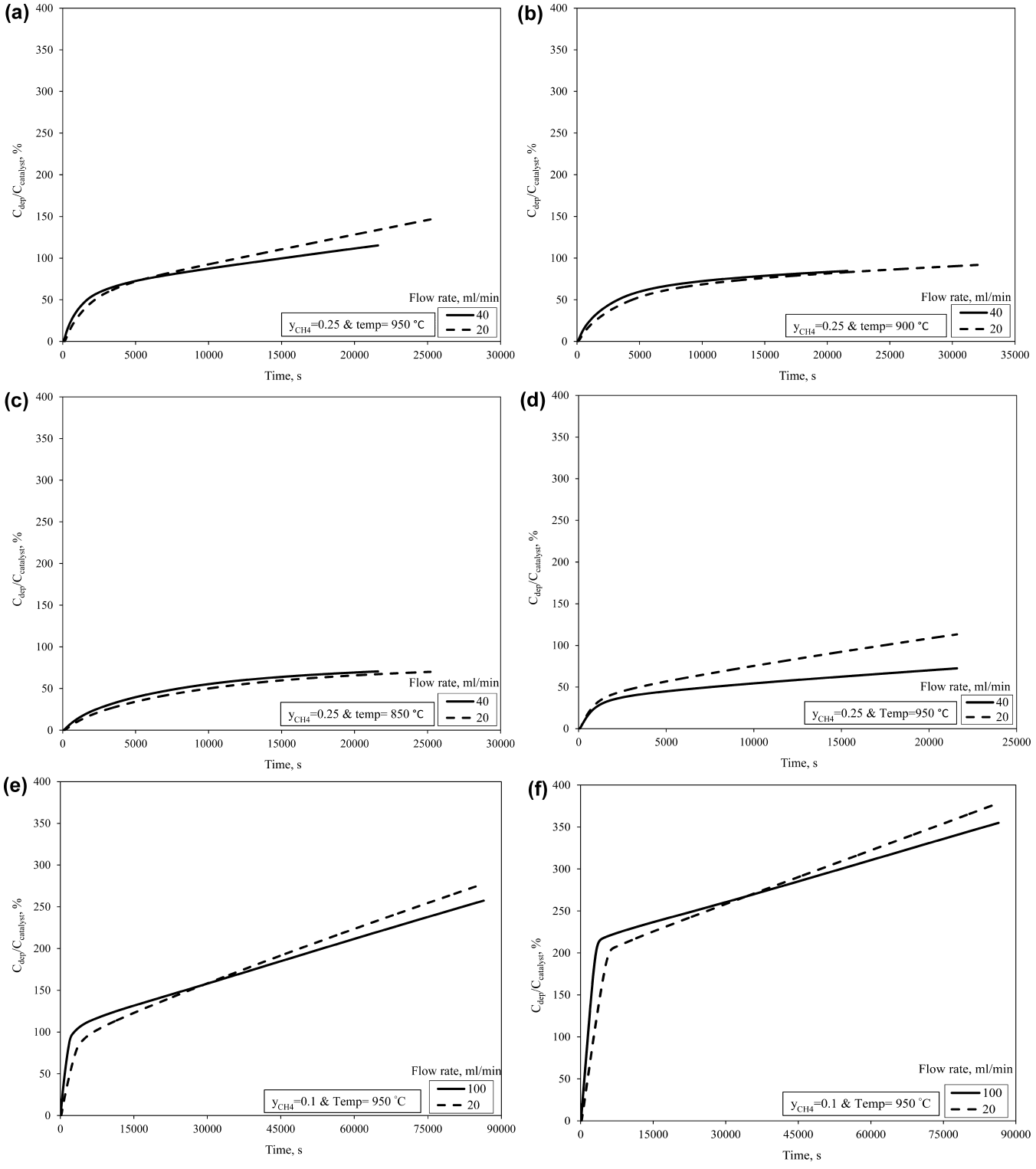

Figure 2. (a) Effect of flow rate on carbon weight gain with Fluka-05105 catalyst. (b) Effect of flow rate on carbon weight gain with Fluka-05105 catalyst. (c) Effect of flow rate on carbon weight gain with Fluka-05105 catalyst. (d) Effect of flow rate on carbon weight gain with Fluka-05120 catalyst.(e) Effect of flow rate on carbon weight gain with CMK-3 catalyst. (f) Effect of flow rate on carbon weight gain with DUT-19 catalyst.

6 h of operation, showing the extreme reduction in absolute reaction rate. This difference in reaction rates and ultimate weight gain might be because of differences in surface structure, single or bimodal pore distribution, the nature of agglomerated carbon formed, and the deactivation mechanism of both samples.

Therefore, there must be a compromise between carbon formation rate and carbon carrying capacity. If an application of the conditions present in Table 3 requires relatively short reaction duration, DUT-19 can be suggested as the better performing catalyst compared to CMK-3 because of its higher average and total hydrogen production rates. However, CMK-3 can be suggested as a catalyst to conduct methane

dx.doi.org/10.1021/ie402195q | Ind. Eng. Chem. Res. 2014, 53, 1741−1753

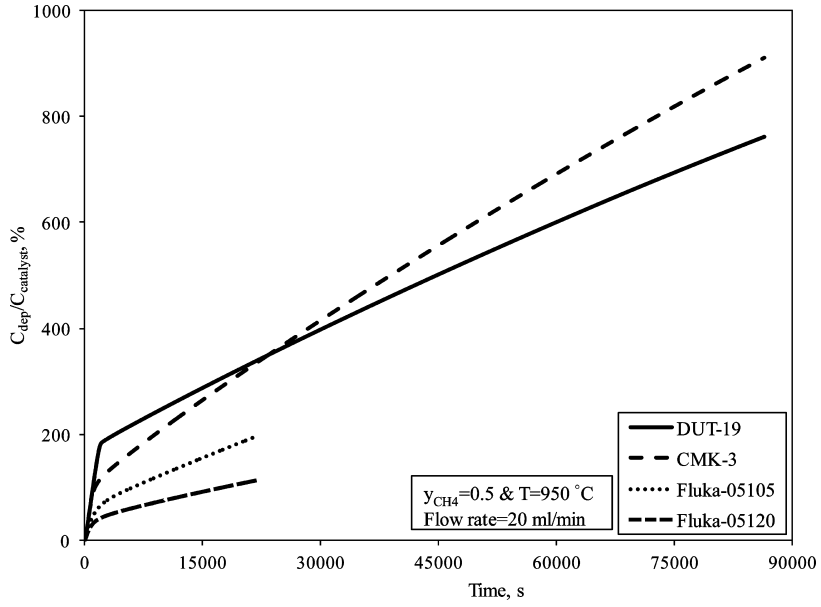

Figure 3. Carbon weight gain with each carbon catalyst (Fluka-05105, Fluka-05120, CMK-3, and DUT-19).

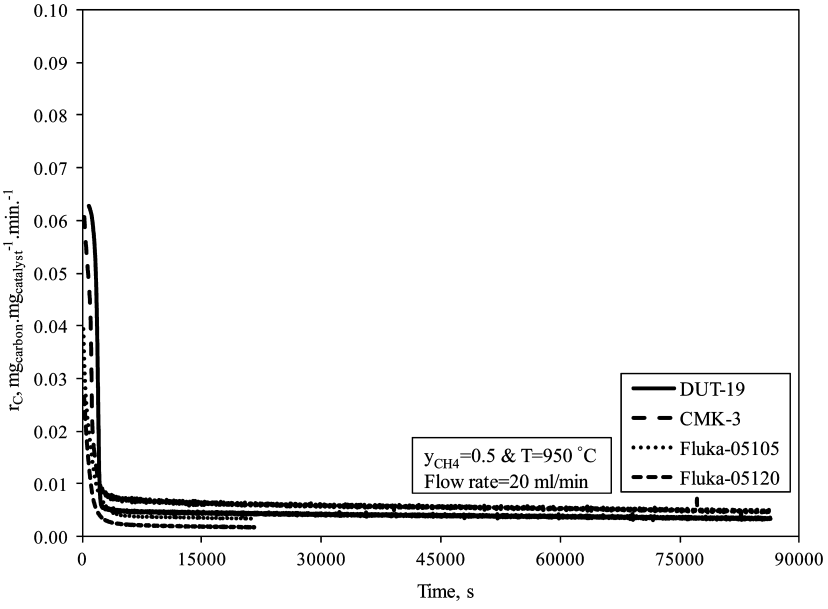

Figure 4. Carbon formation rate with each carbonaceous catalyst (Fluka-05105, Fluka-05120, CMK-3, and DUT-19).

decomposition reaction for longer reaction duration applications with reasonably good reaction rates.

The reason for the lower performance of DUT-19 compared to that of CMK-3 at a reaction temperature of 950 °C and methane partial pressure of 0.5 can be explained as follows. Characterization of our synthesized catalytic samples showed that CMK-3 has a 2D hexagonal structure with a pore diameter of 4.4 nm and surface area of 1400 m^2/g. DUT-19 has a 3D cubic structure with bimodal pores and pore diameters of 1 and 4.6 nm, with a surface area of 2420 m^2/g.[35] The difference in the surface structure and pore size of these catalysts determines the rate of carbon deposition. However, the activities of CMK-3 and DUT-19 were comparable because one pore diameter is approximately the same for both catalysts. For the initial 6 h of operation, the ultimate weight gain was determined to be higher for DUT-19 because the surface area, and therefore the number of active sites within its bimodal pore structure, were higher. After 6 h of operation, the common 4.5 nm pore structure of DUT-19 and CMK-3 may have been filled, whereas the 1 nm pore size of DUT-19 was unfilled. The active sites of the 1 nm pore size of DUT-19 may have been blocked, resulting in a lower reaction rate. After deactivation in the second reaction zone, the reaction rate of all catalysts should either be the equivalent or zero depending on the activity of the agglomerated carbon and the amount of thermally induced reaction. The differences observed in reaction rate for the same reaction conditions across catalysts may be due to a variation in the properties of the carbon formed with each catalyst as a result of catalyst source, origin, preparation, and so forth. Formed carbon may also be participating as a catalyst, resulting in a higher reaction rate for CMK-3.[48]

3.3. Calculation of the Thermodynamically Predicted Carbon Deposition and the Comparison to Experimentally Observed Carbon Formation. Molar flow rates of

dx.doi.org/10.1021/ie402195q | *Ind. Eng. Chem. Res.* 2014, 53, 1741−1753

Table 3. Comparison of Total and Average Hydrogen Production for 6 h of Reaction from Methane Decomposition by Various Carbonaceous Catalysts at Reaction Temperature of 950°C

methane volume, %	catalyst	total hydrogen production, mmol/$g_{catalyst}$	average hydrogen production, mmol/($g_{catalyst}$ min)
50	Fluka-05120	186.584	0.519
	Fluka-05105	326.1127	0.907
	CMK-3	553.374	1.538
		(1517.366)[a]	(1.054)[a]
	DUT-19	560.5	1.56
		(1267.86)[a]	(0.880)[a]
25	Fluka-05120	188.570	0.524
	Fluka-05105	244.010	0.583
	CMK-3	494.334	1.376
		(1222.627)[a]	(0.849)[a]
	DUT-19	498.334	1.389
		(991.161)[a]	(0.688)[a]

[a]For the reaction time of 24 h.

methane ($F_{CH_4,0}$) and inert gas ($F_{He,0}$) of the inlet feed mixture were calculated from the inlet volumetric flow rate (mL/min) and mole or volume fraction of each gas. Assuming time as the basis, this means that $n_{CH_4,0} = F_{CH_4,0}$, $n_{He,0} = F_{He,0}$ and $n_0 = n_{CH_4,0} + n_{He,0}$ (where $n_{CH_4,0}$, $n_{H_2,0}$, and n_0 were the initial moles of methane, hydrogen, and total gas present before the methane decomposition reaction).

Methane decomposes into hydrogen and carbon according to the following reaction:

$$CH_4 \rightarrow C + 2H_2 \quad (1)$$

Chemical reaction thermodynamics defines the relation between the equilibrium constant (K), reaction coordinates (ε), pressure ratio (p/p_0) and initial moles (including inert) as

$$\left(\frac{p}{p_0}\right)^{-1} K = \left\{\frac{(n_{H_2,0} + 2\varepsilon)^2}{(n_0 + \varepsilon)(n_{CH_4,0} - \varepsilon)}\right\} \quad (2)$$

Hydrogen was not present in the feed gas mixture for all of the reactions conducted, so $n_{H_2,0} = 0$. The TGA was operated at ambient pressure, and therefore, $p/p_0 = 1$. As a result, eq 2 reduces to

$$K = \left\{\frac{4\varepsilon^2}{(n_0 + \varepsilon)(n_{CH_4,0} - \varepsilon)}\right\} \quad (3)$$

The equilibrium constant K was calculated from the procedure described in Ozalp et al.[49] Upon rearrangement to obtain the value of reaction coordinate, ε, from the known values of K, n_0, and $n_{CH_4,0}$, the following is obtained:

$$\varepsilon = \frac{-K(n_0 - n_{CH_4,0}) \pm \sqrt{(K(n_0 - n_{CH_4,0}))^2 + 4(4 + K)Kn_0n_{CH_4,0}}}{2(4 + K)} \quad (4)$$

The relation between reaction coordinates and methane conversion found by Lieb and Pereira[50] is given by

$$\varepsilon = \frac{X_{CH_4} n_{CH_4,0}}{\nu_{CH_4}} \quad (5)$$

Therefore X_{CH_4} can be evaluated from the known values $n_{CH_4,0}$, ε, and ν_{CH_4} as

$$X_{CH_4} = \frac{\varepsilon \nu_{CH_4}}{n_{CH_4,0}} \quad (6)$$

where ε is the reaction coordinate, ν_{CH_4} is the stoichiometric coefficient of methane decomposition (=1), X_{CH_4} is methane conversion, and $n_{CH_4,0}$ is the initial moles of methane present.

Once X_{CH_4} was obtained, the molar carbon formation rate can be evaluated by

$$r_{cm} = F_{CH_4,0} X_{CH_4} \quad (7)$$

The amount of carbon deposited over the course of the reaction, CD_T, can be calculated as the product of the molecular weight of carbon (MW_C), reaction time (t) and molar carbon formation rate (r_{cm}) as follows:

$$CD_T = MW_C r_{cm} t \quad (8)$$

This thermodynamically predicted carbon deposition only determines the amount of deposition due to thermal methane cracking and does not take into account the use of a catalyst, the type of catalyst, or catalyst deactivation. Therefore, experimentally observed carbon formation at the end of the catalytic reaction is higher than the thermodynamic calculation. It should be noted that the autocatalyzed reaction might continue even after complete pore blocking of the catalyst. Also, the reaction might run on the outer surface of the blocked catalyst particles. After the very rapid initial blocking, the reaction continues for a long time. These are the main reasons for observing high carbon formation rates. In summary, we can list the reasons to have differences between the theoretical and experimental findings as follows:

i. Carbon formed during methane decomposition can participate in an autocatalytic reaction; therefore, conversion cannot be quantified because carbon is formed as a function of time.
ii. Thermodynamics is time independent. The experimental study shows that methane is fed with a definite flow rate, whereas the carbon formation rate depends on the reaction conditions chosen, such as temperature and concentration. In this view and in agreement with the previous literature, it is seen that methane decomposition is kinetically controlled.
iii. Furthermore, with a carbon catalyzed reaction, there is simultaneous methane decomposition reaction as well as catalyst deactivation taking place at the same time. Therefore, the deactivation mechanism might also change during the course of the reaction. Initial

dx.doi.org/10.1021/ie402195q | Ind. Eng. Chem. Res. 2014, 53, 1741−1753

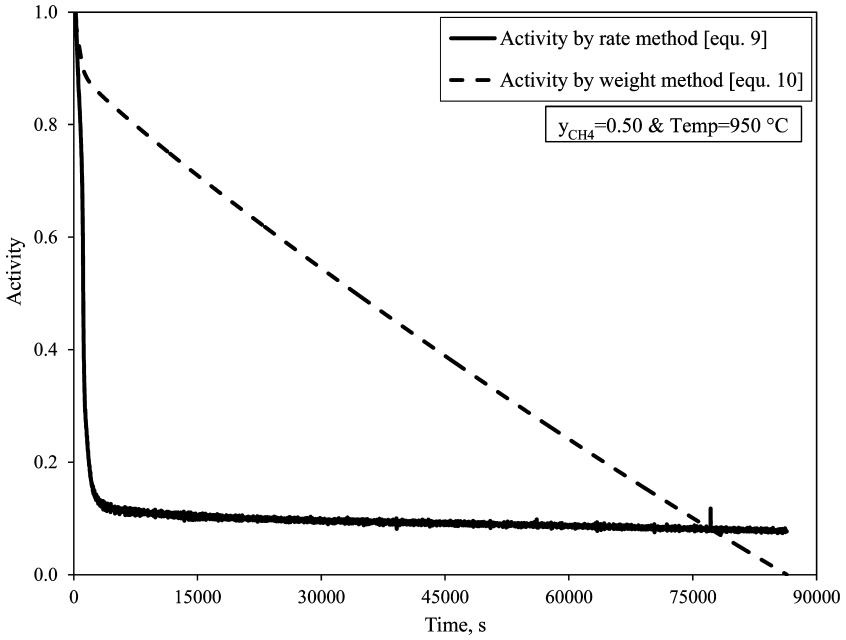

Figure 5. Activity by rate and weight method with CMK-3 catalyst for methane decomposition.

deactivation occurs inside the catalyst pores followed by deactivation on catalysts' external surface as a function of time. Therefore, average conversion during a run can be found by assuming a steady state conversion at various times and summing over time. However, this conversion keeps changing with different experimental durations.

3.4. CATALYTIC ACTIVITY

Activity is defined as ratio of rate of carbon formation at time t to initial rate of carbon formation (r_0).[46] This can be represented mathematically as

$$a(t) = \frac{r_c(t)}{r_0} \tag{9}$$

Where $r_c(t)$ is the rate of carbon formation at time t and r_0 is the initial rate of carbon formation. However, the change of activity based on the carbon formation weight is

$$a(t) = \left[1 - \frac{C(t)_{dep}}{C_{CM}}\right] \tag{10}$$

Where C_{dep} is the weight of carbon deposited at time t, and C_{CM} is the maximum weight of carbon deposited. The activity based on the weight method (eq 10) assumes that deactivation or carbon deposition occurs uniformly on the catalyst surface.[25,47,52]

In eq 9, the initial reaction rate (r_0) is a function of the partial pressure of methane and reaction temperature as observed by Abbas et al.[25] However, the second definition of activity defines C_{CM} as the maximum weight of carbon deposited, which varies with reaction temperature and methane partial pressure. The maximum amount of carbon deposited depends on both reaction temperature and methane partial pressure. As methane partial pressure and reaction temperature increase, the value of C_{CM} will also increase. Therefore, determining a value of C_{CM} for activity plots and calculations was very important. In addition, the plot of C_{dep}/C_{CM} versus activity will always be linear, as per eq 10, immaterial of variations in $C(t)_{dep}$ and C_{CM} in time. However, Abbas and Daud[25,27] did not observe linear data for $C(t)_{dep}/C_{CM}$ versus activity for the various methane partial pressures and reaction temperatures studied. Therefore, C_{CM} was taken as the maximum amount of carbon deposited at the highest temperature and methane partial pressure in their study in order to be able to compare results.

The catalytic activity of CMK-3 calculated via eqs 9 and 10 was plotted as a function of time in Figure 5 in order to compare the results of the two methods. A significant difference in activity was observed in calculations made on the basis of the two aforementioned methods because of the assumptions made in the activity calculations of the weight method. Recent literature describes various methods of determining catalyst activity, such as measuring the conversion of a diluted methane stream in a fixed bed/plug-flow reactor, monitoring outlet hydrogen concentration in a plug-flow reactor, and monitoring the weight gain in time using a TGA.[53−55]

Monitoring weight gain with time has the advantage of eliminating the space limitation issues encountered when using a fixed bed reactor.[54,55]As a result, Rahman et al.[56] selected the TGA for deactivation studies and calculated the catalyst activity in terms of carbon formation rates as shown by eq 9. In this study, activity calculated by carbon formation rate (eq 7) qualitatively matched with those published by Rahman et al.[56] Catalyst activity is a very important variable of interest that must be determined correctly as any error will cascade into the deactivation kinetics calculations in which it is utilized. Therefore, the result of both methods of calculating activity was used to determine deactivation kinetics.

3.5. Deactivation Kinetics. As shown in Figure 1, the carbon formation rate decreased as the reaction proceeded due to carbon deposition on the catalyst surface. The decrease in carbon formation rate illustrates the deactivation of the catalyst due to carbon deposition. Therefore, deactivation and catalyst activity were coupled because the former was the result of the latter; the faster the carbon deposition, the more quickly agglomeration results in a decrease in activity. Carbonaceous catalyst deactivation is one of the most technically challenging problems for the commercial development of hydrogen

dx.doi.org/10.1021/ie402195q | Ind. Eng. Chem. Res. 2014, 53, 1741−1753

Table 4. Deactivation Kinetics for the Methane Decomposition Reaction Determined via Nonlinear Least Square Regression Analysis for Fluka-05120, Fluka-05105, CMK-3 and DUT-19 Carbonaceous Catalyst Samples

	Fluka-05120	Fluka-05105	CMK-3	DUT-19
activity via eq 9		Deactivation Kinetics		
k_{d0}, $(atm^m\ s)^{-1}$	$k_{d0} = 2.78 \times 10^6$	$k_{d0} = 1.08 \times 10^5$	$k_{d0} = 1.12 \times 10^5$	$k_{d0} = 5.62 \times 10^5$
E_d, kJ/mol	$E_d = 192.7$	$E_d = 154.07$	$E_d = 166.08$	$E_d = 181.1$
m, [−]	$m = -0.470$	$m = 0.575$	$m = 0.559$	$m = 0.47$
d, [−]	$d = 0.963$	$d = 0.967$	$d = 0.984$	$d = 0.98$
		Regression Statistics		
	regression coefficient = 0.992	regression coefficient = 0.990	regression coefficient = 0.995	regression coefficient = 0.995
	standard error = 0.074	standard error = 0.081	standard error = 0.084	standard error = 0.072
	number of data points = 28 937	number of data points = 77 851	number of data points = 44 496	number of data points = 44 496
Activity via eq 10		Deactivation Kinetics		
k_{d0}, $(atm^m\ s)^{-1}$	$k_{d0} = 60.4$	$k_{d0} = 50.14$	$k_{d0} = 1.18$	$k_{d0} = 0.0517$
E_d, kJ/mol	$E_d = 102.57$	$E_d = 99.039$	$E_d = 84.64$	$E_d = 49.407$
m, [−]	$m = -0.095$	$m = 0.363$	$m = 0.345$	$m = 0.324$
d, [−]	$d = 0.374$	$d = 0.538$	$d = -0.369$	$d = -0.014$
		Regression Statistics		
	regression coefficient = 0.266	regression coefficient = 0.278	regression coefficient = 0.332	regression coefficient = 0.1407
	standard error = 0.752	standard error = 0.695	standard error = 1.005	standard error = 0.9478
	number of data points = 28 937	number of data points = 77 851	number of data points = 44 946	number of data points = 44 946

produced via methane decomposition.[57,58] Depending on the textural properties and surface chemistry of the catalyst, various mechanisms were proposed for deactivation.[26,45,48,59] Detailed studies of deactivated samples are in progress to determine the mechanism of deactivation for CMK-3, DUT-19, and Fluka samples.

Catalyst deactivation rate can be considered to be a function of reactor temperature, methane partial pressure, and the present state of the catalyst sample.[46] The deactivation rate in terms of the Arrhenius temperature dependency and concentration of gas phase species can be represented as

$$-\frac{da}{dt} = k_d p_{CH_4}^m a^d = k_{d0} e^{-E_d/RT} p_{CH_4}^m a^d \tag{11}$$

where:

$k_d = k_{d0} e^{(-E_d/RT)}$

a is the activity of the catalyst

k_d is the catalyst deactivation rate constant in $(atm^m\ s)^{-1}$

m is a measure of the concentration (p_{CH_4}) dependency

d is the order of deactivation

E_d is the activation energy or temperature dependency of the deactivation in kJ/mol

k_{d0} is the pre-exponential factor in $(atm^m\ s)^{-1}$

There are two possible methods to determine the deactivation kinetic parameters k_{d0}, E_d, m, and d. The first method assumes a simple kinetic form and checks to see if the equation fits the data. In this method, eq 9 is integrated through time for constant values of temperature and methane partial pressure. The result is a catalyst deactivation equation for activity versus time at constant temperature and partial pressure of methane

$$a^{1-d} = 1 - (1 - d) k_d p_{CH_4}^m t \tag{12}$$

Thus, a^{1-d} versus t was plotted for various assumed values of d. The resulting plot yields a straight line with a slope S

$$S = -(1 - d) k_d p_{CH_4}^m \tag{13}$$

The value of d for which the correlation coefficient was highest can be assumed to be the deactivation order. This value should fit data for all methane partial pressures and reaction temperatures chosen. The resulting slope values for each methane partial pressure and reaction temperature will be used to determine the remaining deactivation parameters. Once S was obtained, k_d and m can be obtained by plotting the $\ln(S)$ versus $\ln(p_{CH_4})$ at various reaction temperatures. This can be written as

$$\ln(S) = \ln(-(1 - d) k_d) + m \ln(p_{CH_4}) \tag{14}$$

The slope of the above equation gives the methane concentration dependency m, and the intercept gives the catalyst deactivation rate constant k_d. Different k_d values will be observed at different temperatures. By assuming Arrhenius temperature dependency, the catalyst deactivation rate constant k_d can be expressed as

$$k_d = k_{d0} e^{-E_d/RT} \tag{15}$$

Therefore, a plot of $\ln(k_d)$ versus $1/T$ results in a straight line with a value of $-E_d/R$. The y axis intercept gives the pre-exponential factor.

Using this method to determine deactivation kinetic parameters is less robust, generally providing a poor fit between a^{1-d} versus t for all sets of methane partial pressure and temperature. The deactivation order d obtained by this method was a less versatile value for all reaction conditions. Abbas and Daud[26,27] chose this first method to calculate the deactivation kinetics for methane decomposition. Activity was calculated by the weight method (eq 10) to determine deactivation kinetics.[27]

An alternative method to calculate the deactivation kinetics was used in this study. Once the activity and deactivation rate were determined, eq 11 was directly fit with the experimental data by nonlinear regression analysis. This method gives the all the deactivation kinetic parameters (k_{d0}, E_d, m, d) by considering the simultaneous effect of temperature, methane partial pressure, and deactivation of the catalyst by minimizing the sum of the squared error between the model and

dx.doi.org/10.1021/ie402195q | Ind. Eng. Chem. Res. 2014, 53, 1741−1753

experimental data. This method is considered to be more accurate in obtaining the deactivation parameters because it fits the data best by design.

A recent study by Serrano et al.[48] observed three different carbon deposition rate regimes over the course of methane decomposition reactions for the carbon blacks CB-bp and CB-v and ordered mesoporous carbons CMK-3 and CMK-5. Deactivation phenomena was modeled by considering different functions for deactivation of the initial active sites, autocatalytic behavior of formed carbon, and deactivation of the new active sites by formed carbon deposits occurring during the reaction. A power law model was considered for the autocatalytic effect, whereas a linear or power law function was used for deactivation in Zones 1 and 3 of their study to obtain the deactivation kinetics. Zones 1 and 2 observed by Serrano et al.[48] were not observed in this study, as shown in Figure 2. Therefore, deactivation of the initial carbonaceous catalyst and the autocatalytic effect function was not considered in our model to obtain the deactivation kinetics as shown by eq 11.

Table 4 shows the deactivation kinetics and regression statistics of the nonlinear regression analysis for the various carbon samples studied (Fluka-05120, Fluka-05105, CMK-3, and DUT-19) for methane decomposition. Deactivation kinetics were calculated by evaluating the activity by eqs 9 and 10. From the table, it can be seen that for the same carbonaceous catalyst and experimental data there was a significant difference in the deactivation kinetic parameters. A 5 or 6 orders of magnitude difference in the pre-exponential factor (k_{d0}) was determined by the two methods of calculation. A significant difference in methane concentration dependency (m) and deactivation order (d) were also observed. Furthermore, the regression statics were very poor, and the deactivation kinetics calculated by eq 10 appear to be unrealistic compared to the data. Similar deviations between the two methods were also observed for each catalyst sample studied. The deactivation kinetics calculated from activity determined from the rate method (eq 9) were more appropriate, as the fit to the data was much better. The regression coefficient obtained for activity by eq 9 was above 0.99 for all catalyst samples studied. A deactivation order (d) of approximately 1.0 and a concentration dependency (m) of approximately 0.5 was calculated for all samples. This confirms that deactivation is not occurring uniformly on the catalyst surface. In fact, deactivation is started from the inner pores of the catalyst and moves toward the outer surface. Conversely, Abbas and Daud[27] observed a methane concentration and a deactivation order of 0.5 for palm-shell-based activated carbon. Though this is the second study analyzing the deactivation kinetics of carbonaceous catalysts in a TGA,[48] a more appropriate approach is utilized in order to determine deactivation kinetic parameters.

Shilapuram et al. determined the kinetics for in-house synthesized ordered mesoporous carbons (CMK-3) and carbide derived carbons (DUT-19).[38] Arrhenius energy values of 187 kJ/mol for CMK-3 and 196 kJ/mol for DUT-19 were determined, as well as a reaction order of 0.5 for both catalysts. Table 4 shows that the concentration dependence of methane can be approximated as 0.5 in both reaction kinetics and catalyst deactivation kinetics. The activation energy required for the methane decomposition reaction was higher than the catalytic deactivation of both CMK-3 and DUT-19. This is in agreement with the Abaas and Daud et al.,[25,27] where they observed an activation energy of 210 kJ/mol for methane decomposition and an activation energy for the deactivation of methane decomposition of 194 kJ/mol.

4. CONCLUSIONS

Experiments were conducted in a thermogravimetric analyzer to study catalytic methane decomposition with different carbonaceous catalysts, including activated carbons (Fluka-05120 and Fluka-05105), ordered mesoporous carbons (CMK-3), and ordered carbide-derived carbons (DUT-19). Hydrogen and carbon were produced at various reaction temperatures and feed gas methane mole fractions. The weight of the deposited carbon and the derivative of the carbon deposition rate were determined. Carbon weight gain, carbon formation rate, average hydrogen production, cumulative hydrogen production, and catalytic activity were calculated for each experimental run. The effect of total flow rate was studied with each catalyst. Average and cumulative hydrogen production was compared for each catalyst. Activity was calculated by two definitions, the weight method and the rate method. Deactivation kinetics were obtained by fitting the experimental data via nonlinear regression analysis. The following conclusions were made with respect to the present study:

i. Fluka-05105 demonstrates higher catalytic performance than Fluka-05120.
ii. DUT-19 has the best catalytic properties of all the catalysts studied (Fluka-05120, Fluka-05105, CMK-3, and DUT-19) with higher carbon formation rate, carbon deposited, and average and cumulative hydrogen production.
iii. The effect of flow rates confirms that the system was in a reaction control regime for the particle size and reaction conditions chosen.
iv. A comparison of the thermodynamically predicted carbon formation for the chosen experimental conditions and experimentally observed carbon formation shows that catalytic methane decomposition via carbonaceous catalyst was kinetically controlled as opposed to equilibrium controlled.
v. That there was a large deviation in the activity of the catalysts calculated via the rate method versus the weight method confirmed that deactivation occurred from the pores to outside of the catalyst particle but not uniformly on the catalyst surface.
vi. The deactivation kinetics obtained utilizing the rate method was appropriate for all of the catalysts (Fluka-05120, Fluka-05120, CMK-3, and DUT-19). Results show a deactivation order of approximately 1.0 with a methane concentration dependency of approximately 0.5.
vii. Activation energies of 192, 154, 166, and 181 kJ/mol with pre-exponential factors of 2.78×10^6, 1.08×10^5, 1.12×10^5, and 5.62×10^5 were obtained for Fluka-05120, Fluka-05105, CMK-3, and DUT-19, respectively.

AUTHOR INFORMATION

Corresponding Author

*N. Ozalp. Phone: +974.6686.2832. E-mail: Nesrin.ozalp@qatar.tamu.edu.

Notes

The authors declare no competing financial interest.

■ ACKNOWLEDGMENTS

This research has been funded by National Priorities Research Program of Qatar National Research Fund (QNRF) Project no. NPRP 09-671-2-255.

■ NOMENCLATURE

a = catalyst activity
AC = activated carbon
ACPS = palm-shell-based activated carbon
C_{dep} = amount of carbon deposited on catalyst, mg
$C_{Catalyst}$ = initial amount of catalyst, mg
C_{CM} = maximum weight of carbon deposited
CB = carbon black
CFD = computational fluid dynamics
d = order of deactivation
E_d = activation energy of deactivation, kJ/mol
$F_{CH_4,0}$ = molar flow rate of methane in the feed gas, mol/h
$F_{He,0}$ = molar flow rate of helium in the feed gas, mol/h
K = equilibrium constant
k_d = catalyst deactivation rate constant, $(atm^m\ s)^{-1}$
k_{d0} = pre-exponential factor, $(atm^m\ s)^{-1}$
m = measure of the methane concentration (p_{CH_4}) dependency
$n_{CH_4,0}$ = initial moles of methane in the feed
$n_{H_2,0}$ = initial moles of hydrogen in the feed
$n_{He,0}$ = initial moles of helium in the feed
n_0 = initial moles of feed mixture
P = pressure
P_0 = atmospheric pressure
p_{CH_4} = partial pressure of methane
R = gas constant
r_0 = initial rate of methane decomposition, $mg_{carbon}\ (mg_{catalyst}\ min)^{-1}$
r_c = carbon formation rate, $mg_{carbon}\ (mg_{catalyst}\ min)^{-1}$
r_{cm} = molar carbon formation rate, mol_{carbon}/h
S = slope of catalyst deactivation equation in time
SEM = scanning electron microscopy
T = temperature
X_{CH_4} = methane conversion
XRD = X-ray diffraction
y_{CH_4} = methane mole fraction in the feed gas

Greek Symbols

ε = reaction coordinates

■ REFERENCES

(1) Muradov, N. Z.; Veziroglu, T. N. "Green" path from fossil-based to hydrogen economy: An overview of carbon-neutral technologies. *Int. J. Hydrogen Energy* **2008**, *33*, 6804.
(2) Holladay, J. D.; Hu, J.; King, D. L.; Wang, Y. An overview of hydrogen production technologies. *Catal. Today* **2009**, *139*, 244.
(3) Steinfeld, A. Solar thermochemical production of hydrogen-a review. *Solar Energy* **2005**, *78*, 603.
(4) Shilapuram, V.; Jaya Krishna, D.; Ozalp, N. Residence time distribution and flow field study of aero-shielded solar cyclone reactor for emission-free generation of hydrogen. *Int. J. Hydrogen Energy* **2011**, *36*, 13488.
(5) Rodat, S.; Abanades, S.; Flamant, G. Experimental evaluation of indirect heating tubular reactors for solar methane pyrolysis. *Int. J. Chem. React. Eng.* **2010**, *8*, 1.
(6) Kogan, A.; Israeli, M.; Alcobi, E. Production of hydrogen and carbon by solar thermal methane splitting. IV. Preliminary simulation of a confined tornado flow configuration by computational fluid dynamics. *Int. J. Hydrogen Energy* **2007**, *32*, 4800.
(7) Maag, G.; Zanganeh, G.; Steinfeld, A. Solar thermal cracking of methane in a particle flow reactor for the co-production of hydrogen and carbon. *Int. J. Hydrogen Energy* **2009**, *34*, 7676.
(8) Ozalp, N.; Shilapuram, V. Step-by-step methodology of developing a solar reactor for emission-free generation of hydrogen. *Int. J. Hydrogen Energy* **2010**, *35*, 4484.
(9) Li, Y.; Li, D.; Wang, G. Methane decomposition to CO_2-free hydrogen and nano-carbon material on group 8−10 base metal catalysis: A review. *Catal. Today* **2011**, *162*, 1.
(10) Piao, L.; Li, Y.; Chen, J.; Chang, L.; Lin, J. Y. S. Methane decomposition to carbon nanotubes and hydrogen on an alumina supported nickel aerogel catalyst. *Catal. Today* **2002**, *74*, 145.
(11) Yeheskel, J.; Epstein, M. Thermolysis of methane in a solar reactor for mass-production of hydrogen and carbon nanomaterials. *Carbon* **2011**, *49*, 4695.
(12) Pinilla, J. L.; Torres, D.; Lazaro, M. J.; Suelves, I.; Moliner, R.; Canadas, I.; Rodriguez, J.; Vidal, A.; Martinez, D. Metallic and carbonaceous-based catalysts performance in the solar catalytic decomposition of methane for hydrogen and carbon production. *Int. J. Hydrogen Energy* **2012**, *37*, 9645.
(13) Sharif, H.; Sharif, A. Z.; Mohamed, R.; Sesha, T. S. Kinetic studies on catalytic decomposition of methane to hydrogen and carbon over Ni/TiO_2 catalyst. *Ind. Eng. Chem. Res.* **2004**, *43*, 4864.
(14) Muradov, N.; Smith, F.; T-Raissi, A. Catalytic activity of carbons for methane decomposition. *Catal. Today* **2005**, *102−103*, 225.
(15) Muradov, N.; Smith, F.; Huang, C.; T-Raissi, A. Auto-thermal catalytic pyrolysis of methane as a new route to hydrogen production with reduced CO_2 emissions. *Catal. Today* **2006**, *116*, 281.
(16) Suelves, I.; Lázaro, M. J.; Moliner, R.; Pinilla, J. L.; Cubero, H. Hydrogen production by methane decarbonization: carbonaceous catalysts. *Int. J. Hydrogen Energy* **2007**, *32*, 3320.
(17) Lee, K. K.; Han, G. Y.; Yoon, K. J.; Lee, B. K. Thermocatalytic hydrogen production from the methane in a fluidized bed with activated carbon catalyst. *Catal. Today* **2004**, *93−95*, 81.
(18) Ryu, B. H.; Lee, S. Y.; Lee, D. H.; Han, G. Y.; Lee, T. J.; Yoon, K. J. Catalytic characterization of various rubber-reinforcing carbon blacks in decomposition of methane for hydrogen production. *Catal. Today* **2007**, *123*, 303.
(19) Bai, Z.; Li, W.; Bai, J.; Li, B.; Chen, H. The effects of textural properties and surface chemistry of activated carbon on its catalytic performance in methane decomposition from hydrogen production. *Energy Sources, Part A* **2012**, *34*, 1145.
(20) Gatica, J. M.; Gomez, D. M.; Harti, S.; Vidal, H. Monolithic honey comb design applied to carbon material for catalytic methane decomposition. *Appl. Catal., A* **2013**, *458*, 21.
(21) Fidalgo, B.; Menendez, J. A. Carbon materials as catalysts for decomposition and CO_2 reforming of methane: A review. *Chin. J. Catal.* **2011**, *32*, 207.
(22) Muradov, N. Z. CO_2-free production of hydrogen by catalytic pyrolysis of hydrocarbon fuel. *Energy Fuels* **1998**, *12*, 41.
(23) Muradov, N. Catalysis of methane decomposition over elemental carbon. *Catal. Commun.* **2001**, *2*, 89.
(24) Muradov, N.; Smith, F.; Bokerman, G. Methane activation by non-thermal plasma generated carbon aerosols. *J. Phys. Chem. C* **2009**, *113*, 9737.
(25) Abbas, H. F.; Daud, W. M. A. W. Thermo-catalytic decomposition of methane using palm shell based activated carbon: kinetic and deactivation studies. *Fuel Process. Technol.* **2009**, *90*, 1167.
(26) Abbas, H. F.; Daud, W. M. A. W. Hydrogen production by thermocatalytic decomposition of methane using a fixed bed activated carbon in a pilot scale unit: apparent kinetic, deactivation and diffusional limitation studies. *Int. J. Hydrogen Energy* **2010**, *35*, 12268.
(27) Abbas, H. F.; Daud, W. M. A. W. Deactivation of palm shell-based activated carbon catalyst used for hydrogen production by thermocatalytic decomposition of methane. *Int. J. Hydrogen Energy* **2009**, *34*, 6231.
(28) Abbas, H. F.; Baker, I. F. Thermocatalytic decomposition of methane using activated carbon: Studying the influence of process

parameters using factorial design. *Int. J. Hydrogen Energy* **2011**, *36*, 8985.
(29) Pinilla, J. L.; Suelves, I.; Lazaro, M. J.; Moliner, R. Kinetic study of the thermal decomposition of methane using carbonaceous catalysts. *Chem. Eng. J.* **2008**, *138*, 301.
(30) Suelves, I.; Pinilla, J. L.; Lázaro, M. J.; Moliner, R. Carbonaceous materials as catalysts for decomposition of methane. *Chem. Eng. J.* **2008**, *140*, 432.
(31) Serrano, D. P.; Botas, J. A.; Pizarro, P.; Guil-Lopez, R.; Gomez, G. Ordered mesoporous carbons as highly active catalysts for hydrogen production by CH_4 decomposition. *Chem. Commun.* **2008**, *48*, 6585.
(32) Serrano, D. P.; Botas, J. A.; Guil-Lopez, R. H_2 production from methane pyrolysis over commercial carbon catalysts: kinetic and deactivation study. *Int. J. Hydrogen Energy* **2009**, *34*, 4488.
(33) Serrano, D. P.; Botas, J. A.; Fierro, J. L. G.; Guil-Lopez, R.; Pizarro, P.; Gomez, G. Hydrogen production by methane decomposition: Origin of the catalytic activity of carbon materials. *Fuel.* **2010**, *89*, 1241.
(34) Botas, J. A.; Serrano, D. P.; Guil-Lopez, R.; Pizarro, P.; Gomez, G. Methane catalytic decomposition over ordered mesoporous carbons: a promising route for hydrogen production. *Int. J. Hydrogen Energy* **2010**, *35*, 9788.
(35) Botas, J. A.; Serrano, D. P.; Pizarro, P.; Gomez, G. Ordered mesoporous carbons as catalyst with remarkable activity and stability for hydrogen production without CO_2 emissions by CH_4 decomposition. *Proc. World Hydrogen Energy Conf., 18th*; Stolten D., Ed.; Wiley-VCH: Weinheim, Germany, 2010; pp *243*−*248*.
(36) Ozalp, N.; Shilapuram, V. Characterization of activated carbon for carbon laden flows in a solar reactor (Paper no. AJTEC2011-44381). *Proc. ASME/JSME Therm. Eng. Jt. Conf., 8th*; ASME: New York, 2011.
(37) Shilapuram, V.; Ozalp, N. Carbon catalyzed methane decomposition for enhanced solar thermal cracking (Paper no. ESFuelcell2011-54644). *ASME Int. Conf. Energy Sustainability, Proc., 5th*; ASME: New York, 2011.
(38) Shilapuram, V.; Ozalp, N.; Oschatz, M.; Borchardt, L.; Kaskel, S. Hydrogen production from catalytic decomposition of methane over ordered mesoporous carbons (CMK-3) and carbide-derived carbon (DUT-19). *Carbon*, accepted for publication.
(39) Krawiec, P.; Kockrick, E.; Borchardt, L.; Geiger, D.; Corma, A.; Kaskel, S. Ordered mesoporous carbide derived carbons: Novel materials for catalysis and adsorption. *J. Phys. Chem. C* **2009**, *113*, 7755.
(40) Kockrick, E.; Schrage, C.; Borchardt, L.; Klein, N.; Rose, M.; Senkovska, I.; Kaskel, S. Ordered mesoporous carbide derived carbons for high pressure gas storage. *Carbon* **2010**, *48*, 1707.
(41) Oschatz, M.; Kockrick, E.; Rose, M.; Borchartdt, L.; Klein, N.; Senkovska, I.; Freudenberg, Y.; Korenblit, G.; Yushin, G.; Kaskel, S. A cubic ordered, mesoporous carbide-derived carbon for gas and energy storage applications. *Carbon* **2010**, *48*, 3987.
(42) Zhou, H.; Zhu, S.; Hibino, M.; Honma, I.; Ichihara, M. Lithium storage in ordered mesoporous carbon (CMK-3) with high reversible specific energy capacity and good cycling performance. *Adv. Mater.* **2003**, *15*, 2107.
(43) Ozalp, N.; Ibrik, K.; Al-Meer, M. Kinetic and heat transfer analysis of carbon catalyzed solar cracking process. *Energy* **2013**, *15*, 74.
(44) Foggler, H. S. *Elements of chemical reaction engineering*, 4th ed.; Pearson Education, Inc.: Upper Saddle River, NJ, 2006.
(45) Kim, M. H.; Lee, E. K.; Jun, J. H.; Kong, S. J.; Han, G. Y.; Lee, B. K.; Lee, T. J.; Yoon, K. J. Hydrogen production by catalytic decomposition of methane over activated carbons: kinetic study. *Int. J. Hydrogen Energy* **2004**, *29*, 187.
(46) Levenspeil, O. *Chemical Reaction Engineering*, 3rd ed., John Wiley & Sons: New York; 1999.
(47) Yoon, Y. H.; Park, N. K.; Chang, W. C.; Lee, T. J.; Hur, T.; Lee, B. G.; Baek, Y. S. Hydrogen production by pyrolysis of natural gas: thermodynamic analysis. *Trans. Korea Hydrogen Energy Soc.* **2002**, *13* (1), 42.
(48) Serrano, D. P.; Botas, J. A.; Pizarro, P.; Gomez, G. Kinetic and autocatalytic effects during the hydrogen production by methane decomposition over carbonaceous catalysts. *Int. J. Hydrogen Energy* **2013**, *38*, 5671.
(49) Ozalp, N.; Shilapuram, V. Step-by-step methodology of developing a solar reactor for emission-free generation of hydrogen. *Int. J. Hydrogen Energy* **2010**, *35*, 4484.
(50) Leib, T. M.; Pereira, C. J. Reaction Kinetics. In Green, D. W., Perry, R. H., Eds.; *Perry's Chemical Engineers' Handbook*, 8th ed.; McGraw-Hill: New York, 2008; p 7-1−7-39.
(51) Kim, M. H.; Lee, E. K.; Jun, J. H.; Han, G. Y.; Kong, S. J.; Lee, B. K.; Lee, T. J.; Yoon, K. J. Hydrogen production by catalytic decomposition of methane over activated carbons: deactivation study. *Korean J. Chem. Eng.* **2003**, *20*, 835.
(52) Oudar, J.; Wise, H. *Deactivation and Poisoning of catalysts*; Marcel Dekker: New York, 1985.
(53) Shah, N.; Panjala, D.; Huffman, G. P. Hydrogen production by catalytic decomposition of methane. *Energy Fuels* **2001**, *15*, 1528.
(54) Zhang, T.; Amiridis, M. D. Hydrogen production via the direct cracking of methane over silica-supported nickel catalysts. *Appl. Catal., A* **1998**, *167*, 161.
(55) Aiello, R.; Fiscuc, J. E.; Loye, H. C.; Amiridis, M. D. Hydrogen production via the direct cracking of methane over Ni/SiO_2 catalyst deactivation and regeneration. *Appl. Catal., A* **2000**, *192*, 227.
(56) Rahman, M. S.; Croiset, R. E.; Hudgins, R. R. Catalytic decomposition of methane for hydrogen production. *Top. Catal.* **2006**, *37*, 137.
(57) Abanades, A.; Rubbia, C.; Salmieri, D. Technical challenges for industrial development of hydrogen production based on methane cracking. *Energy* **2012**, *46*, 359.
(58) Abanades, A.; Rubbia, C.; Salmieri, D. Thermal cracking of methane into hydrogen for a CO_2-free utilization of natural gas. *Int. J. Hydrogen Energy* **2013**, *20*, 8491.
(59) Lázaro, M. J.; Pinilla, J. L.; Suelves, I.; Moliner, R. Study of the deactivation mechanism of carbon blacks used in methane decomposition. *Int. J. Hydrogen Energy* **2008**, *33*, 4101.